ADVANCED FUNCTIONAL MATERIALS
www.afm-journal.de

Freestanding $BaTiO_3$-Au Vertically Aligned Nanocomposite toward Flexible Multi-Sensing Platform

*Benson Kunhung Tsai, Jialong Huang, Ya-Ching Yu, Meng Hao Lee, Benjamin Thomas Stegman, Emiliano Joseph Flores, Patrick Zhang Tong, Ke Xu, Shiyu Zhou, Jianan Shen, Jiawei Song, Yizhi Zhang, Lia Stanciu, Wenzhuo Wu, Xinghang Zhang, and Haiyan Wang**

Flexible and wearable sensors show enormous potential for personalized healthcare devices by real-time monitoring of an individual's health. Typically, a single functional material is selected for one sensor to sense a particular physical signal while multiple materials will be selected for multi-mode sensing. Vertically aligned nanocomposites (VANs) have recently demonstrated various material combinations and novel coupled multifunctionalities that are hard to achieve in any single-phase material alone, including multiphase multiferroics, magneto-optic coupling, and strong magnetic and optical anisotropy. Integrating these novel VANs into wearable sensors shows enormous potential in multi-mode sensing owing to their multifunctional nature. In this work, the transfer of VANs onto polydimethylsiloxane as a novel flexible chemical and pressure sensor is demonstrated. For this demonstration, the classical $BaTiO_3$ -Au VAN with combined plasmonic and piezoelectric properties is used to demonstrate a multi-sensing mechanism. A thin water-soluble buffer of $Sr_3Al_2O_6$ serves as a buffer layer for the epitaxial growth and transfer process. The electrical output based on the piezoelectric responses and identifying 4-mercaptobenzoic acid by surface-enhanced Raman spectroscopy reveal great potential for free-standing VANs in a wearable multifunctional sensing platform.

1. Introduction

Different from the traditional electronic devices that are bulky and rigid, wearable electronics are light and flexible. This shows great potential in personal health monitoring and electronic device applications, such as flexible field-effect transistors, wearable biosensors, and electronics for human–machine interfaces.[1,2] Considering the very versatile physical properties of oxides, various freestanding oxide-based thin films have been demonstrated for different electronic devices, such as nanomechanical resonators, dielectric gates for field effect transistors, and multifunctional devices based on 2D-3D heterostructure.[3–6] Specifically, freestanding $BaTiO_3$ (BTO) thin film for a micromechanical resonator with ferroelectric hysteresis been observed with the resonance frequency. Freestanding $SrTiO_3$ has been applied as the gate material for the field effect transistor.[5,7] Integrating $La_{0.7}Sr_{0.3}MnO_3$ to MoS_2 to demonstrate the photodiode device with magnetic responses.[8] Interestingly, perovskite oxides with ferroelectric or antiferroelectric properties, which are known to be rigid in nature, show surprising deformability when they are freestanding thin films.[9–11] Some of the oxides even show different physical properties after the transfer, such as freestanding $NaNbO_3$ exhibiting a thickness-dependent antiferroelectric-to-ferroelectric property transition,[12] and $BiFeO_3$ exhibiting unexpected giant polarization and

B. K. Tsai, J. Huang, Y.-C. Yu, B. T. Stegman, E. J. Flores, P. Z. Tong, K. Xu, S. Zhou, J. Shen, J. Song, Y. Zhang, L. Stanciu, X. Zhang, H. Wang
School of Materials Engineering
Purdue University
West Lafayette, IN 47907, USA
E-mail: hwang00@purdue.edu

The ORCID identification number(s) for the author(s) of this article can be found under https://doi.org/10.1002/adfm.202418004

DOI: 10.1002/adfm.202418004

M. H. Lee, W. Wu
School of Industrial Engineering
Purdue University
West Lafayette, IN 47907, USA

L. Stanciu
School of Biomedical Engineering
Purdue University
West Lafayette, IN 47907, USA

H. Wang
School of Electrical and Computer Engineering
Purdue University
West Lafayette, IN 47907, USA

tetragonality when down to the 2D limit.[13] Overall, these novel properties on freestanding oxides present even more device potentials than those on rigid oxide substrates.

To process flexible oxide thin film-based devices, different methods have been demonstrated. Lee et al. has demonstrated by using the laser lift-off process to obtain a flexible PZT piezoelectric nanogenerator for pressure-based sensing.[14] Using another method, BTO could also achieve as a flexible thin film. BTO was direct deposited on the Mica substrate, after exfoliating the mica to a certain thickness, a flexible BTO thin film can be obtained.[15] Utilizing post-deposition transfer is an alternative method to fabricate the electronic device. Han et al. demonstrated using $Sr_3Al_2O_6$ (SAO) as a buffer layer to grow BTO first, then fabricate a 2D/3D/2D heterostructure for a high energy density capacitor.[16] Sun et al. integrated freestanding BTO on silicon to demonstrate a ferroelectric domain wall memory device.[17] A work by Han et al. shows the freestanding bilayer oxide thin film for the skyromion-like polar domain.[18] Most of the oxide-based device demonstrations have focused on single-phase thin film or multilayer thin film with one functionality. Recently, multifunctional vertically aligned nanocomposites (VAN) have been deposited onto mica to demonstrate as a flexible oxide-based electronic device.[19]

VAN is a unique group of nanostructures with a nanopillar-in-matrix form, have recently drawn great interest because of their strong coupling along vertical interfaces, strong out-of-plane anisotropy, and novel multi-functionalities that are hard to achieve in a single phase alone.[19] Up-to-date, many oxide-oxide VANs, some oxide-metal VANs,[20,21] and nitride-metal VANs[22,23] have been reported. Novel properties including multiferroic properties,[24] superior vertical ionic transport properties,[25] perpendicular exchange bias,[26] strong hyperbolic properties,[27] tunable plasmonic properties,[28] magnetic anisotropy,[22] magneto-optical coupling,[29] etc., have been demonstrated. Especially the recent demonstrated oxide-metal VANs as hybrid plasmonic metamaterials present novel tailorable plasmonic and hyperbolic behavior depending on the metal selections and pillar density tuning. By combining the optical properties of metal and the functionality of oxide, these new VANs present great potential in multi-mode sensing schemes and thus could be considered as new multi-functional materials candidates for flexible electronics.

In this work, a new class of freestanding thin films, namely the oxide-metal VAN thin films, has been demonstrated. More specifically, nearly all the oxide-metal VAN films require a single crystalline oxide substrate and high deposition temperature for epitaxial growth. This has limited the potential of integrating the unique multifunctional VAN films for practical device applications since most of the devices were grown on Si or other substrates and cannot withstand very high processing temperatures. This free-standing VAN demonstration could allow the integration of multifunctional VANs in future devices. The second highlight of the work is the potential application of oxide-metal VAN for multi-functional sensing applications.

Furthermore, changes in the deposition parameters result in structural changes, which allows the physical properties to be tuned.[30] Thus, a desired thin film with tailored physical properties can be used for specific sensing applications. BTO-Au VAN is selected considering the piezoelectric properties of BTO and plasmonic Au for the proposed multifunctional sensor as illustrated in **Figure 1**. BTO-Au VAN is selected considering the piezoelectric properties of BTO and plasmonic Au for the proposed multifunctional sensor as illustrated in Figure 1. The multifunctional sensor includes piezoelectric sensing and surface-enhanced Raman spectra for chemical sensing. The thin film transfer process was enabled by a water-soluble buffer of $Sr_3Al_2O_6$ (SAO) as discussed in the method section and illustrated in Figure 1. After optimization, very few or no wrinkles were found on the transferred film surface on PDMS. Further characterization to compare before and after transferring the multifunctional thin film includes high-resolution X-ray diffraction (XRD), high-resolution scanning transmission electron microscopy (STEM), and atomic force microscopy (AFM) analysis. The piezoelectric electric response under different bending strains and surface-enhanced Raman spectroscopy for chemical sensing has been demonstrated. This new VAN-based multifunctional flexible sensor presents great potential for applying complex oxide composites for flexible lightweight device platforms.

2. Results and Discussion

BTO-Au nanocomposite thin films were deposited onto the SAO buffer layer, then transferred on to a flexible substrate such as PDMS. BTO was selected as the matrix phase due to its piezoelectric responses to external stress.[3,11,31] Au was selected to enhance the Raman signal for chemical analysis. Previously, BTO-Au VAN thin film with phase separation was shown to grown on STO (001).[32] Specifically, during the VAN growth, the two phases separate and nucleate on the substrate as the matrix and the pillars depending on their phase composition ratio. Then the adatoms continue to grow as the separated matrix and pillars form the VAN structure. The in-plane distribution of the two phases is based on the strain compensation model,[33]where the in-plane lattice mismatch between the VAN film and the substrate is based on the lattice parameters of the combined two phases and the substrate. Preferably phase A with a slightly larger lattice and phase B with a slightly smaller lattice than that of the substrate lattice will result in a better in-plane strain matching of the VAN.[30] For the case of the BTO-Au VAN growth on the SAO buffer in this work, it is more complicated due to the large lattice parameter of SAO. The lattice constant of a cubic unit cell for SAO is a = 15.844 Å ($a/4$ = 3.961 Å), which matches with four times of STO (001) (a = 3.905 Å) substrate lattice ($4\times a_{STO}$ = 15.620 Å).[34,35] Thus BTO-Au VAN does not follow the strain compensation model. The XRD $\theta-2\theta$ result for the direct growth of BTO-Au VAN on SAO is shown in Figure S1a (Supporting Information). The result shows there are no obvious film peaks other than the STO (001) substrate and SAO (008), which suggests the BTO-Au VAN thin film does not epitaxially grow on top of the SAO buffer. This might be due to the effective lattice of the BTO-Au with BTO (a = 4.83 Å)[36] and Au (a = 4.072 Å)[20] does not match well with the lattice of SAO ($a/4$ = 3.961 Å).[30] Thus, a thin BTO buffer layer has been deposited on top of the SAO buffer layer to establish the effective in-plane strain for BTO-Au VAN thin film growth on top. After incorporating the BTO buffer layer the XRD result in **Figure 2b** reveals the as-grown heterostructure shows the peaks for BTO (002), which is similar to the

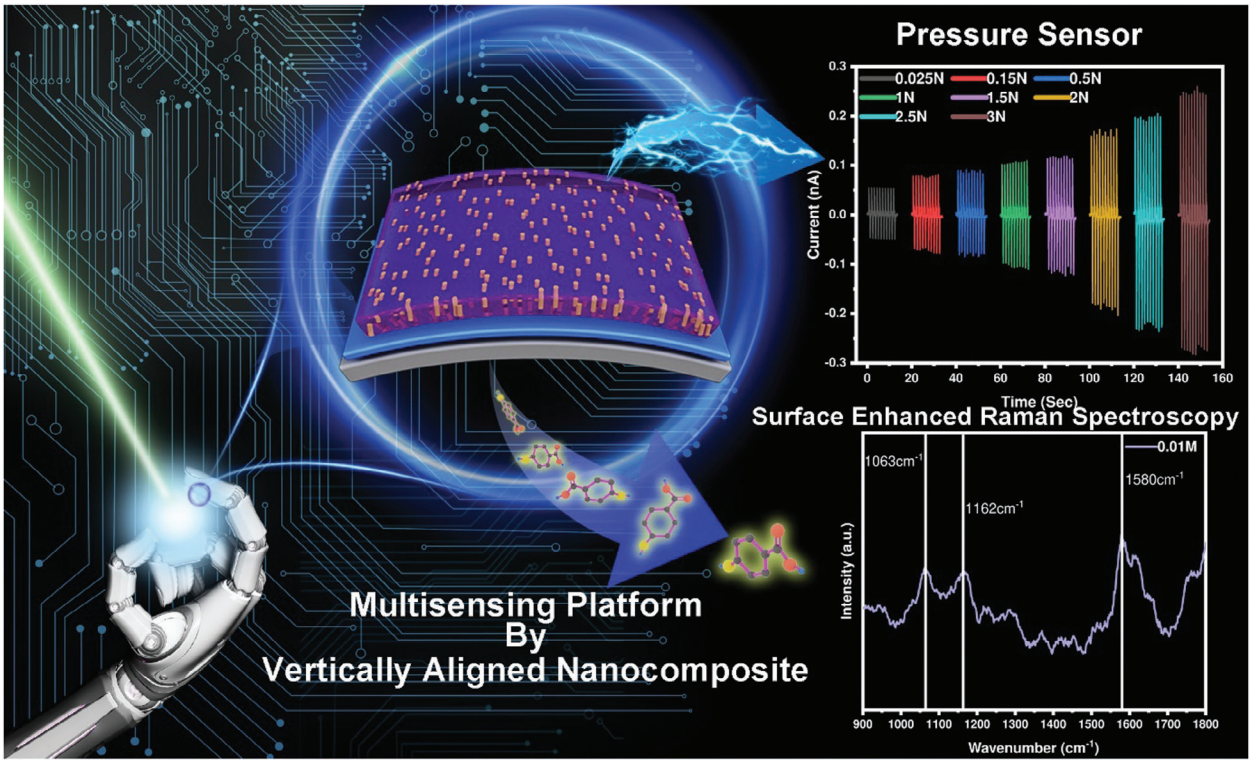

Figure 1. Schematic illustration on the multi-sensing platform by freestanding vertically aligned nanocomposite.

previously reported BTO-Au VAN thin film on STO (001).[32,37] In addition, the SAO (008) peak is clearly shown in the XRD pattern, which means the SAO has grown highly textured on STO (001). However, the Au (111) peak that is shown in the previous result does not show here.[32] This might due to the low concentration of the Au nanopillars in the sample. To further characterize the nanostructure of the thin film, cross-sectional STEM, and selected area diffraction pattern (SAED) were conducted to confirm the morphology of the BTO-Au thin film. Figure 2c shows the result of the SAED, suggesting a cube-on-cube epitaxy. The overall heterostructure of SAO/BTO/BTO-Au VAN thin film is shown in Figure S2a (Supporting Information) by a low magnification STEM image. In addition, the corresponding STEM-EDS result is shown in Figure S2b (Supporting Information). The overall nanostructure shows Au nanopillars within the BTO matrix. It is noted that some of the Au nanopillars did not continuously grow from the bottom to the top, as shown in Figure 2d. To further confirm the Au nanostructure within the BTO matrix, an enlarged image of a representative area was shown in Figure 2e. It suggests that the Au nanopillars are indeed formed within the matrix. To confirm the composition distribution of the VAN thin film structure, STEM-EDS mapping was conducted and is shown in Figure 2f. STEM-EDS images confirm that the element for the nanopillar structure is Au, and the matrix corresponds to BTO. The STEM and STEM-EDS result confirms the growth of BTO-Au VAN.

Transferring oxide thin films using SAO as a buffer layer has been demonstrated previously.[3,38,39] However, transferring oxide-metal-based VAN thin film remains unexplored and requires optimization. PDMS-based transfer has been widely used for transferring perovskite oxide thin films[3,5,40] and thus was also selected for this demonstration. Different transfer methods with PDMS have been adopted here and the overall results are shown in **Figure 3**. To make sure the SAO is fully dissolved, all transfer methods ensure STO substrate naturally falls off and the thin film adheres to PDMS before lifting out from the water. The first method is schematically shown in Figure 3a, where additional weight is added on the top to make sure that the film and PDMS are in good contact. The resulting transferred film is shown in Figure 3d,g via optical microscopy (OM) and scanning electron microscopy (SEM) imaging, respectively. The resulting transferred film with weight during the process is in pieces as shown in Figure 3d. Additional OM results show more wrinkles forming than the other two transfer methods in Figure S3a–c (Supporting Information). This suggests the film was under stress during the dissolution process, and the stress has been released after taking the transferred thin film out from the water.[41,42] In addition, there are some cracks forming, which might due to the defect generation in the thin film[40,43] or the fact that the thin film cannot compensate the sudden force during the retraction process of PDMS after the weight is lifted. The second method is shown in Figure 3b, where the entire film is immersed in DI water with the substrate on top. The film was stuck onto the PDMS by the natural adhesion force from the PDMS. Some cracks still formed after the dissolving process, which can be observed by OM and SEM in Figure 3e,h. In addition, Figure S2d–f (Supporting Information) shows there are more cracks with this transfer method. Nonetheless, a no-wrinkle and crack-free thin film sample was not obtained. Last, the sample was placed on top of the PDMS gently without any additional

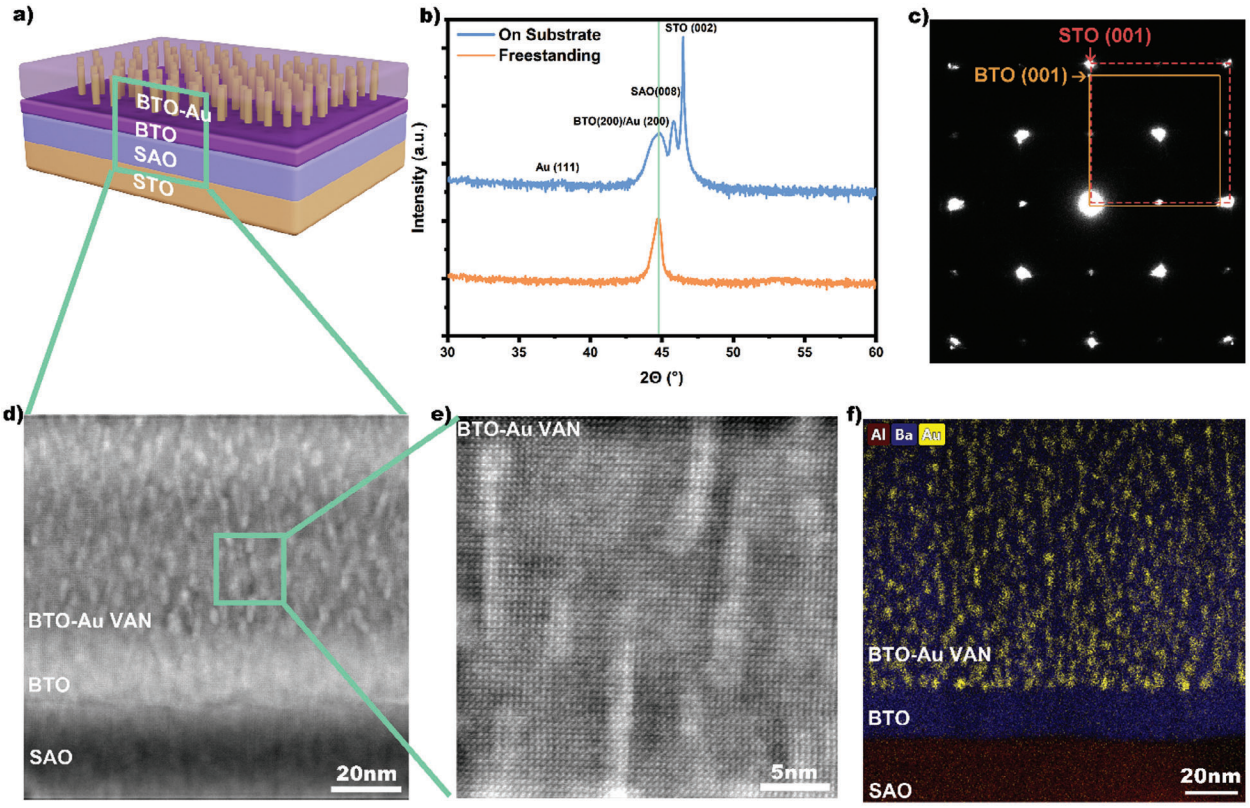

Figure 2. Microstructure characterization. a) Schematic illustration on the overall nanostructure. b) X-ray diffraction result of the overall VAN thin film before and after the dissolution process. c) The selected area diffraction pattern for the as-grown thin film. d,e) high angle annular dark field scanning transmission electron microscopy (HAADF-STEM) image for the VAN nanostructure. f) the corresponding STEM-EDS image of (d).

pressure being applied to the film. Once the sample is placed on the PDMS, the adhesion force of the PDMS allows the thin film to stick on top. The entire stack is then floating on top of water, where the heterostructure thin film is still in the water for dissolution. Figure 3c shows the schematic of the process. The resulting OM image in Figure 3f shows that the number of wrinkles and cracks is significantly reduced. However, the after-transferred VAN thin film still forms additional wrinkles and cracks, which are shown in Figure S2d–i (Supporting Information). To further ensure the crack-free region has no microcrack forming, SEM was conducted. The image from SEM is shown in Figure 3i, suggesting there is no microcrack shown over a large area. Furthermore, AFM images in Figure S3 (Supporting Information) also ensure the low-density wrinkles and the flat region within the film that discussed above. After obtaining the AFM image for both regions, three different lines of height profiles are obtained in the graph to illustrate the wrinkle area has a significant height difference compared to the flat region.

As discussed above, multiple different single-phase perovskite oxides showed superior flexibility based on prior studies.[11,44] In addition, nanostructure Au has been selected as an electrode for flexible electronics.[45] Thus, it is interesting to investigate the flexibility of the transferred oxide-metal VAN films. To examine the flexibility of the VAN thin film, this film has been attached onto PDMS/PET and an in situ mechanical straining test under SEM was conducted. The motor of the in situ mechanical test has moved with the range from 1 mm to 10 mm. The overall schematic on how the film was gradually bent, is shown in **Figure** 4a. The size of the thin film on top is 5 mm × 5 mm and PDMS/PET is 5 cm × 5 cm. To ensure the thin film is bending downward, a slight initial bending has been applied to it. The overall result is shown in Figure 4b–e, where the bending distance increases from 1mm to 10mm. It shows the number of wrinkles increases gradually to compensate for the bending strain. Since, PET is a rigid thermoplastic, and PDMS is a flexible stretchable elastomer. PDMS can then generate wrinkles during the bending process. Thus, PDMS might be the reason that there are more wrinkles generated. Additional high-magnification SEM for the two largest bending distances is shown in Figure 4f,g. The resulting image shows there are no cracks being generated even under this large bending strain. In addition, Figure S4 (Supporting Information) shows the SEM image of the thin film after recovering from the bending test. The result shows an excellent recoverability, where no obvious crack formation.

The thickness of the BTO-Au thin film is 228 nm here, which is ≈100 nm thicker than previously reported transferred perovskite oxides.[10,12,41,44,46] The underlying deformability of flexible BTO-Au VAN films could be attributed to the combined effects including the domain switching in BTO, the coupled deformation between Au and BTO interface, and the Au nanostructures. The mechanical properties for ferroelectric thin film, such as BTO, were

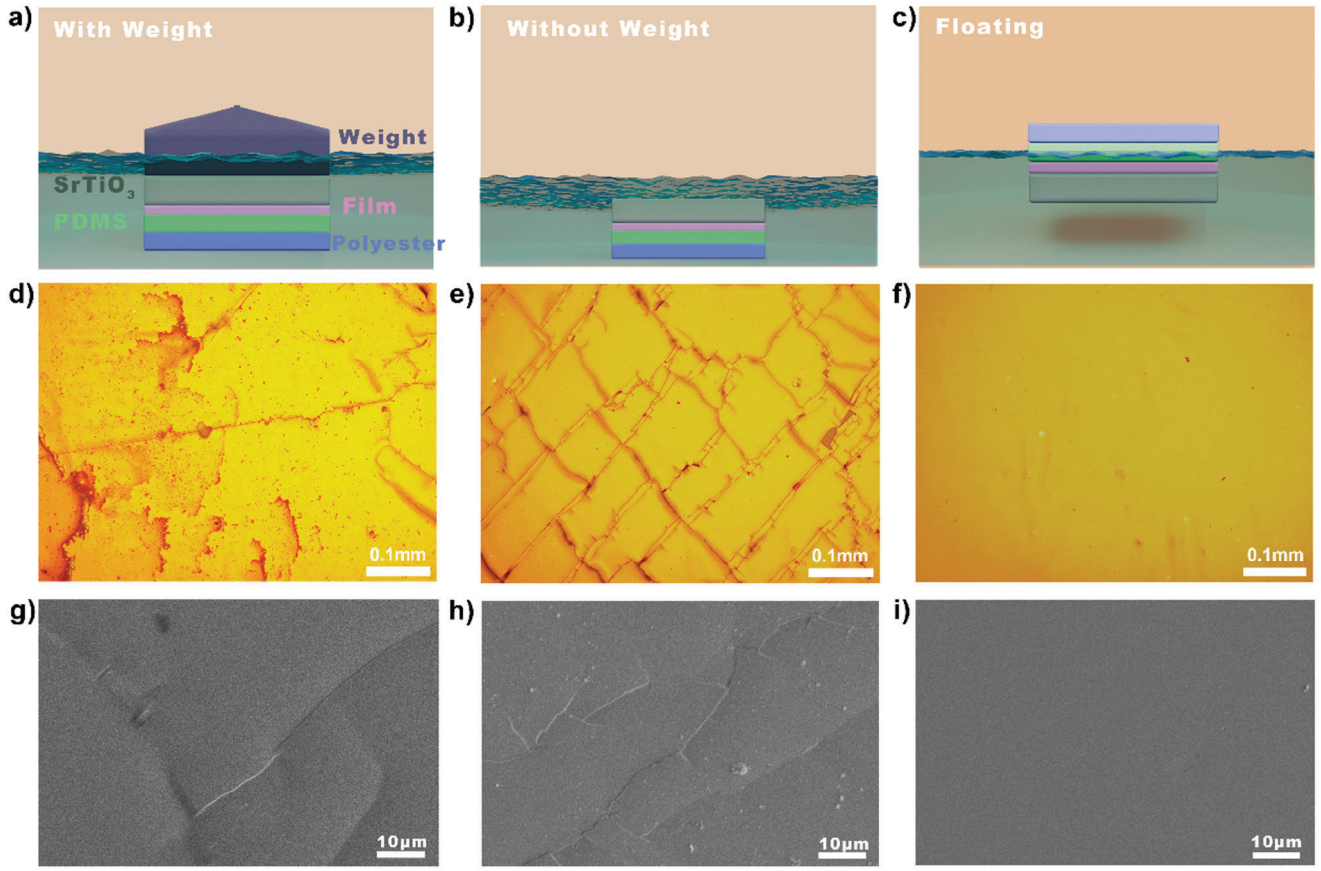

Figure 3. The overall transfer method. a–c) schematic illustration on the dissolution process. d–f) shows the optical microscopy image for the result of the dissolution. g–i) Scanning electron microscopy images to examine any additional microcrack. Clearly, the floating method shows the best transfer results without any obvious crack formation.

previously reported to be largely dependent on domain state and phases.[10,11] In addition, the mechanical force can induce ferroelastic domain switching.[47] By declamping the thin film from the substrate, it has been shown that the ferroelastic domain switch can become faster than those on rigid substrates.[48,49] In addition, Au is known to be a ductile metal with both elastic and plastic deformability, which is widely used in flexible electronic as an electrode.[45,50,51] Thus, Au nanowires could potentially facilitate the plastic deformation in the BTO matrix. Such ductile behavior has been previously reported in TiN-Au and TaN-Au VANs.[23] The detailed mechanism could be explored in the future, such as mechanical testing by AFM[12] and in situ TEM to understand the mechanical mechanism at the BTO and Au interface.

The mechanical and physical properties have been explored on selected polymer and oxide-metal VAN thin films, which could potentially apply as a wearable multi-sensing platform. One of the applications for the piezoelectric property is a force sensor,[31,52] while the application of the plasmonic property is surface-enhanced Raman spectroscopy (SERS) for chemical sensing.[53] In addition, multifunctional sensors has been applied in human–machine interfaces to understand the chemical and physical of the surrounding environment.[54] Considering the multifunctionality of the VAN thin film, which could potentially be considered as a new material for multifunctional sensors as illustrated in **Figure 5**. BTO-Au VAN thin film could allow the selection of the sensing mode depending on the need. Furthermore, it can potentially miniaturize the overall device size. First, we have tested the piezoelectric property under different forces applied, as shown in Figure 5a. All forces have been monitored by force gauge and applied under the speed of 1 mm sec^{-1}. After calculating the average current outputs, the current density increases from 0.0022 to 0.0098 nA mm^{-2} as the amount of the force that applied to the film increases as shown in Figure 5b. The sensitivity for the piezoelectric-based pressure sensor is calculated in supporting information.[55,56] Based on the calculation, the sensitivity of the sensor is determined to be 0.71 k Pa^{-1}, such performance has compared with others as shown in Table S1 (Supporting Information). In addition, the stability test for piezoelectric response under fixed bending distance (20 mm) and speed (1 mm s^{-1}), which is shown in Figure S5 (Supporting Information). The resulting piezoelectric stability test shows the electric output is stable over 15 mins. Next, we measured the Raman response of a selected chemical on the transferred VAN films to explore its SERS effects. Since the film was deposited in a sequence of BTO and then BTO-Au, the Au cannot be exposed to the surface after being transferred on the PDMS. One additional step on the transfer method is adopted here. After the thin film

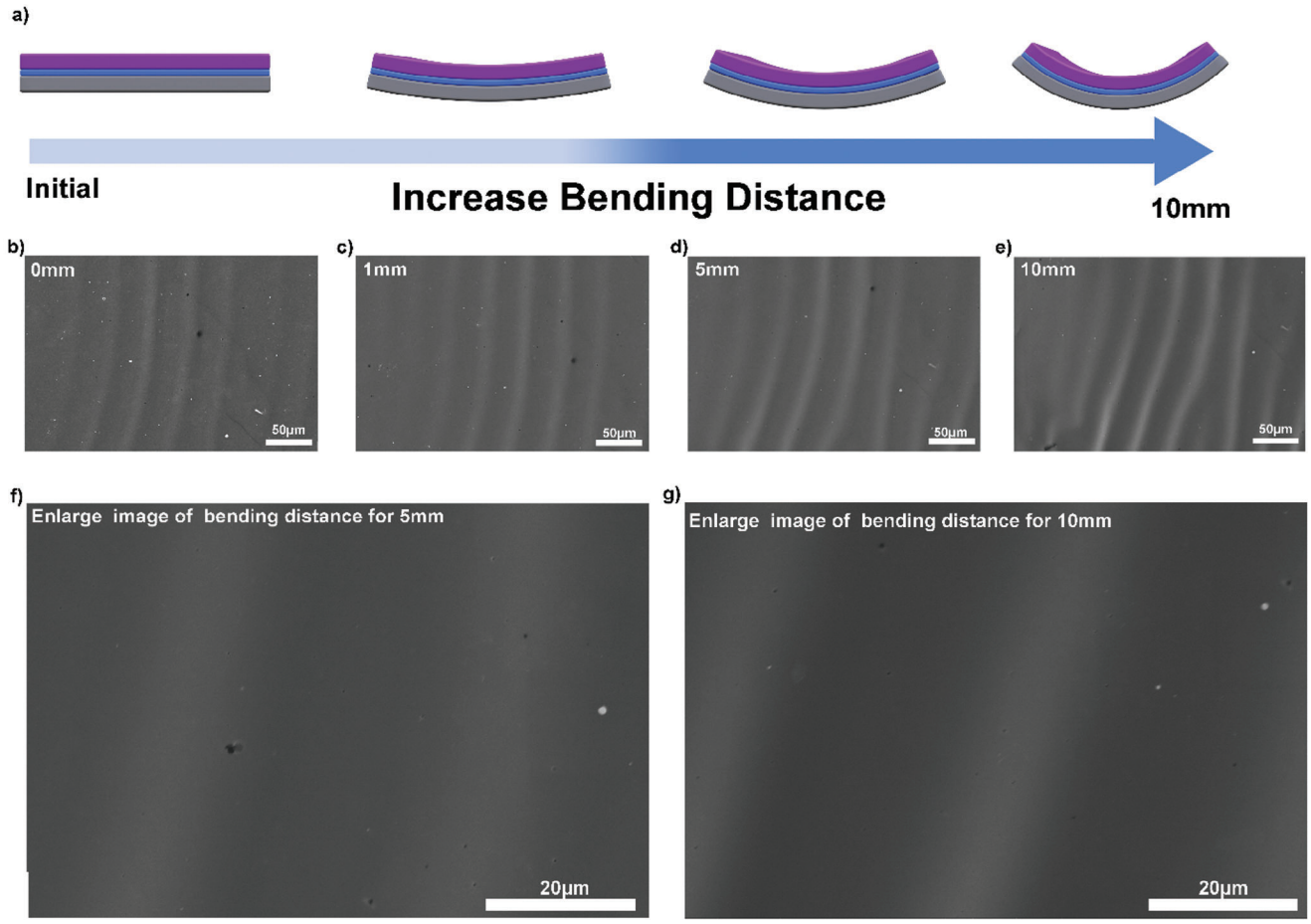

Figure 4. In situ SEM image. a) schematic illustration on the mechanical bending. b–e) shows the condition of the film. The overall result shows there are no additional cracks created during the process. f,g) shows the magnified image for (d,e), which shows the bending process doesn't generate microcrack.

was on the PDMS, the thin film was then transfer on to a new Si substrate to allow the exposure of the top BTO-Au VAN layer.[5,39] To demonstrate the SERS effect for the film, 4-mercaptobenzoic acid (4-MBA) is selected as the chemical and the concentration is 0.01 M.[57] In addition, a transferred BTO will serve as a blank to ensure the plasmonic property of Au can enhance the Raman signal. The result of the pure BTO film is shown in Figure S7 (Supporting Information) without any signature peak for 4-MBA. Figure 5c shows the Raman spectrum results for BTO-Au thin film with 4-MBA. The distinct peak are assigned as follows: $\nu(CC)_{ring}$ ring-breathing modes (1063 cm^{-1}), $\nu(CC)_{ring}$ ring stretching (1580 cm^{-1}), $\delta(CH)$ bends (1165 cm^{-1}).[58] Thus, it indeed shows the SERS effect can be observed in the VAN thin film. Here, a new potential multi-sensing application for oxide-metal VAN has been demonstrated. It is noted that the pressure sensing and chemical sensing were measured separately in this work as the demonstration of multifunctional sensing schemes using one material platform. The possible interactions between the two sensing schemes were not explored but could be an interesting future direction. For example, a potential future work could be to explore the SERS effects on chemical sensing based on different strain states upon bending of the flexible BTO-Au VAN thin films. Furthermore, there are potential concerns about the large size of the Raman spectroscopy tools could potentially limit the chemical sensing applications. It is noted that in recent work,[59] SERS has been demonstrated as an alternative method for sweat sensing applications by using a handheld Raman spectroscopy to detect chemical signals. This demonstration suggests that it is possible to implement the proposed VAN free-standing films and a small-scale Raman spectroscopy tool for the proposed chemical sensing applications.

Here the multifunctional sensor within one VAN complex nanocomposite thin film has been demonstrated. Such VAN shows a huge potential for miniaturization of the sensor device. In addition, the self-powered piezoelectric could provide a potential for low-power consumption sensors. Some additional oxide-metal-based VAN could potentially provide alternative sensing applications for multi-sensing platforms. For example, magnetic-based VANs such as $La_{0.7}Sr_{0.3}MnO_3$-Au[21] thin film could potentially sense the magnetic field and perform chemical sensing because of the ferromagnetic LSMO and plasmonic Au. The simple materials combination changes and morphology tuning provide an opportunity to broaden the sensing modes and adjust the sensitivity of the sensors. The other example of a multifunctional sensor is combining the BTO with ferromagnetic Fe[60] to sense the magnetic field and the pressure at the same

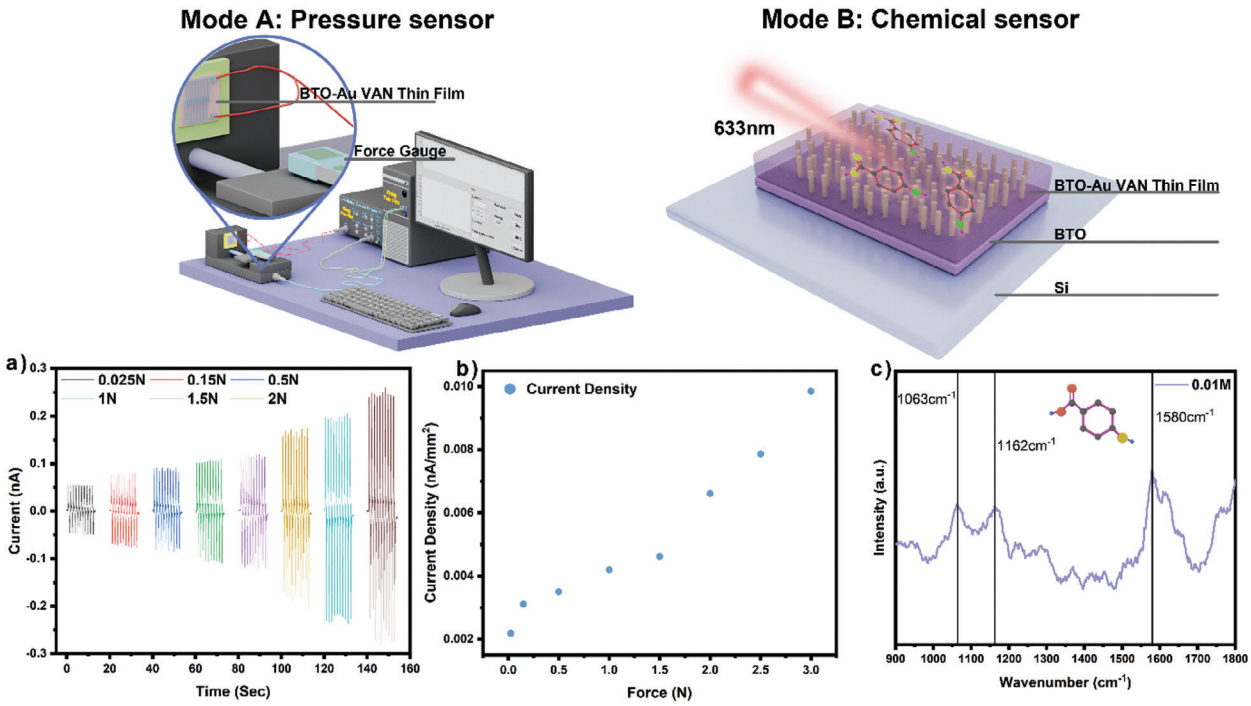

Figure 5. Demonstration on multifunctional sensor. a) piezoelectric output under different forces b) average current density under different forces c) surface-enhanced Raman spectroscopy for 4-mercaptobenzoic acid (4-MBA).

time. However, there should be some improvements for the VAN nanostructure as well as the thin film transfer process. To maximize the signal from the SERS effect, it is important to create a "hot spot" for the chemical to stay in. Thus, a more detailed nanostructure design should be considered. Next, it is important to improve the piezoelectric responses. The BTO thin film on the plastic substrate can reach high current density, which might provide a better signal-to-noise ratio.[31] The metal that is incorporated into the dielectric matrix thin film can indeed decrease the piezoelectric responses. However, a multilayer thin film with two different VAN layers may improve the signal of piezoelectric responses.[61] Such improvement may lead to better pressure sensitivity. Last, engineering the lattice parameters of SAO could result in a better quality of thin film. A recent study shows close lattice matching with the lattice parameters of STO substrate by doping Ca into SAO, which will generate less crack for the freestanding thin film.[62] Such doped SAO buffer could also be explored for the transfer of BTO VAN thin films for reduced lattice strain and crack generation during the transfer process.

3. Conclusion

A flexible and multifunctional sensor of freestanding BTO-Au VAN thin film has been successfully demonstrated. Detailed material characterizations including XRD, STEM, and STEM-EDS revealed high-quality growth of VAN thin film on SAO buffered STO substrates. After film transfer, an in situ mechanical tension test under SEM was conducted and showed that BTO-Au VAN thin film presents excellent flexibility and recoverability upon cyclic bending. Utilizing the multifunctionality nature of the free-standing BTO-Au thin film, a multifunctional sensor to detect the force and the chemical applied has been achieved. This work demonstrates the great potential of transferred free-standing oxide-metal VAN thin films as future multifunctional sensing platforms.

4. Experimental Section

Synthesis of Multifunctional Thin Film and Thin Film Transferring Method: The $Sr_3Al_2O_6$ target was prepared by a mixture of stochiometric amounts of $SrCO_3$ and Al_2O_3. Both $BaTiO_3$ and $Sr_3Al_2O_6$ (SAO) were sintered in a conventional tube furnace at 1300 °C for 10 hours. $BaTiO_3$-Au thin film was grown on $SrTiO_3$ (001) substrates by using pulsed laser deposition with KrF excimer laser (248 nm, Coherent). SAO was deposited at a temperature of 850 °C in an oxygen partial pressure of 50 mtorr with laser energy of 420 mJ and a laser frequency of 2 Hz. $BaTiO_3$-Au thin film was deposited at a temperature of 650 °C in an oxygen partial pressure of 50 mtorr with laser energy of 420 mJ and a laser frequency of 2 Hz. The sample was immediately cooled to room temperature at 10 °C min^{-1}.

The multifunctional vertically aligned nanocomposite thin film was placed on top of a poly(dimethylsiloxane) (PDMS) stamp (Gel-Pak, PF-40-X4) without additional pressure. Then placed the sample into DI water till SAO was fully dissolved.

Material Characterization: All thin films were examined using XRD (PANalytical Empyrean). All scanning transmission electron microscopy (STEM) samples were prepared using diamond lapping film (Allied High Tech. Products Inc.) for mechanical grinding followed by dimpling to thin down the sample. Once the desired thickness was obtained, argon-ion milling using a Gatan Precision Ion milling system was used for final polishing. All STEM analysis was carried out using a Thermo Fisher Scientific TALOS 200X TEM operated at 200 kV.

Device Characterization: An in situ mechanical bending test was performed using a Kammrath–Weiss tensile machine equipped in a Teneo scanning electron microscope (FEI). Once the desired distance was

reached, the microstructure of the thin film was examined by the scanning electron microscope.

Surface-enhanced Raman spectroscopy was performed using a Renishaw InVia. The spectrum was obtained at 633 nm with 10% power of the laser. The 4-mercaptobenzoic acid (Millipore Sigma) was resuspended at 0.01 M in ethanol. Once the solution was fully mixed, one drop of 10 µL of the mixed solution was applied onto the thin film.

Electrical measurements were performed using an electrometer (Keithley 6514) and a low-current preamplifier (Stanford Research System, SR570). All statistical data were summarized from three tests, with a total of 10 peaks from each test applied to calculate average outputs and standard deviation. A linear motor was used as the external force to drive the device (maximum speed ranging from 1 to 20 m s^{-1}, with acceleration and deceleration both equal to 1 m s^{-2}).

Supporting Information

Supporting Information is available from the Wiley Online Library or from the author.

Acknowledgements

This work was supported by the U.S. National Science Foundation (DMREF-2323752). Y.Z. and H.W. acknowledge the support from the U.S. National Science Foundation for microscopy analysis (DMR-2016453). J.S. and H.W. acknowledge the support from the U.S. Department of Energy, Office of Science, Basic Energy Sciences under Award (DE-SC0020077) for the effort on device testing. S.Z. and H.W. acknowledge the support from the U.S. Office of Naval Research (N00014-22-1-2160) for the bulk synthesis of target materials and powder processing. This paper describes objective technical results and analysis. Any subjective views or opinions that might be expressed in the paper do not necessarily represent the views of the U.S. Department of Energy, the U.S. National Science Foundation, or the United States Government.

Conflict of Interest

The authors declare no conflict of interest.

Author Contributions

B.K.T. and J.H. contributed equally to this work. B.K.T., J.H., and H.W. dealt with the conceptualization, methodology, investigation, formal analysis, validation, visualization, and writing the original draft. B.K.T., J.S., Y.Z., and H.W. dealt with nanostructure characterization, formal analysis, and writing the review and editing. B.K.T. and J.H. dealt with optical property characterization. B.T.S., J.S., J.S., and Y.Z. dealt with TEM images acquisition and analysis. B.T.S, E.J.F., and P.Z.T. dealt with in situ mechanical testing. M.H.L. and W.W. dealt with piezoelectric testing. Y.C.Y. and L.S. dealt with chemical preparation for SERS effect testing. X.Z. and H.W. dealt with the conceptualization, methodology, writing the review and editing, project administration, funding acquisition, supervision, and resources.

Data Availability Statement

The data that support the findings of this study are available in the supplementary material of this article.

Keywords

Au nanopillars, freestanding thin films, piezoelectric, surface-enhanced Raman spectroscopy, vertically aligned nanocomposites, wearable sensors

Received: September 24, 2024
Revised: December 16, 2024
Published online: January 23, 2025

[1] M. Bariya, H. Y. Y. Nyein, A. Javey, *Nat. Electron.* **2018**, *1*, 160.
[2] A. K. Katiyar, A. T. Hoang, D. Xu, J. Hong, B. J. Kim, S. Ji, J.-H. Ahn, *Chem. Rev.* **2024**, *124*, 318.
[3] M. Lee, J. R. Renshof, K. J. van Zeggeren, M. J. A. Houmes, E. Lesne, M. Šiškins, T. C. van Thiel, R. H. Guis, M. R. van Blankenstein, G. J. Verbiest, A. D. Caviglia, H. S. J. van der Zant, P. G. Steeneken, *Adv. Mater.* **2022**, *34*, 2204630.
[4] D. Davidovikj, D. J. Groenendijk, A. M. R. V. L. Monteiro, A. Dijkhoff, D. Afanasiev, M. Siskins, M. Lee, Y. Huang, E. van Heumen, H. S. J. van der Zant, A. D. Caviglia, P. G. Steeneken, *Commun. Phys.* **2020**, *3*, 163
[5] J.-K. Huang, Y.i Wan, J. Shi, J.i Zhang, Z. Wang, W. Wang, N.i Yang, Y. Liu, C.-H.o Lin, X. Guan, L. Hu, Z.i-L. Yang, B.o-C. Huang, Y.a-P. Chiu, J. Yang, V. Tung, D. Wang, K. Kalantar-Zadeh, T. Wu, X. Zu, L. Qiao, L.-J. Li, S. Li, *Nature.* **2022**, *605*, 262
[6] A. J. Yang, L. Wu, Y. Liu, X. Zhang, K. Han, Y. Huang, S. Li, X. J. Loh, Q. Zhu, R. Su, C.-W. Nan, X. R. Wang, *Adv. Mater.* **2023**, *35*, 2302620
[7] A. J. Yang, K. Han, K. Huang, C. Ye, W. Wen, R. Zhu, R. Zhu, J. Xu, T. Yu, P. Gao, Q. Xiong, X. Renshaw Wang, *Nat. Electron.* **2022**, *5*, 233.
[8] A. J. Yang, L. Wu, Y. Liu, X. Zhang, K. Han, Y. Huang, S. Li, X. J. Loh, Q. Zhu, R. Su, C.e-W. Nan, X. Renshaw Wang, *Adv. Mater.* **2023**, *35*, 2302620.
[9] Y. Guo, B. Peng, G. Lu, G. Dong, G. Yang, B. Chen, R. Qiu, H. Liu, B. Zhang, Y. Yao, Y. Zhao, S. Li, X. Ding, J. Sun, M. Liu, *Nat. Commun.* **2024**, *15*, 4414.
[10] B. Peng, R.-C. Peng, Y.-Q. Zhang, G. Dong, Z. Zhou, Y. Zhou, T. Li, Z. Liu, Z. Luo, S. Wang, Y. Xia, R. Qiu, X. Cheng, F. Xue, Z. Hu, W. Ren, Z.-G. Ye, L.-Q. Chen, Z. Shan, T. Min, M. Liu, *Sci. Adv.* **2020**, *6*, eaba5847.
[11] G. Dong, S. Li, M. Yao, Z. Zhou, Y.-Q. Zhang, X. Han, Z. Luo, J. Yao, B. Peng, Z. Hu, H. Huang, T. Jia, J. Li, W. Ren, Z.-G. Ye, X. Ding, J. Sun, C.-W. Nan, L.-Q. Chen, J. Li, M. Liu, *Science* **2019**, *366*, 475 .
[12] R. Xu, K. J. Crust, V. Harbola, R. Arras, K. Y. Patel, S. Prosandeev, H. Cao, Y.-T. Shao, P. Behera, L. Caretta, W. J. Kim, A. Khandelwal, M. Acharya, M. M. Wang, Y. Liu, E. S. Barnard, A. Raja, L. W. Martin, X. W. Gu, H. Zhou, R. Ramesh, D. A. Muller, L. Bellaiche, H. Y. Hwang, *Adv. Mater.* **2023**, *35*, 2210562 .
[13] D. Ji, S. Cai, T. R. Paudel, H. Sun, C. Zhang, L.u Han, Y. Wei, Y. Zang, M. Gu, Y.i Zhang, W. Gao, H. Huyan, W. Guo, D.i Wu, Z. Gu, E. Y. Tsymbal, P. Wang, Y. Nie, X. Pan, *Nature.* **2019**, *570*, 87.
[14] K.-I. Park, J. H. Son, G.-T. Hwang, C. K. Jeong, J. Ryu, M. Koo, I. Choi, S. H. Lee, M. Byun, Z. L. Wang, K. J. Lee, *Adv. Mater.* **2014**, *26*, 2514 .
[15] D. Y. Hyeon, K.-I. Park, *Energy Technol.* **2019**, *7*, 1900638.
[16] S. Han, J. S. Kim, E. Park, Y. Meng, Z. Xu, A. C. Foucher, G. Y. Jung, I. Roh, S. Lee, S. O. Kim, J.-Y. Moon, S.-I. Kim, S. Bae, X. Zhang, B.-I. Park, S. Seo, Y. Li, H. Shin, K. Reidy, A. T. Hoang, S. Sundaram, P. Vuong, C. Kim, J. Zhao, J. Hwang, C. Wang, H. Choi, D.-H. Kim, J. Kwon, J.-H. Park, et al., *Science* **2024**, *384*, 312.
[17] H. Sun, J. Wang, Y. Wang, C. Guo, J. Gu, W. Mao, J. Yang, Y. Liu, T. Zhang, T. Gao, H. Fu, T. Zhang, Y. Hao, Z. Gu, P. Wang, H. Huang, Y. Nie, *Nat. Commun.* **2022**, *13*, 4332.
[18] L.u Han, C. Addiego, S. Prokhorenko, M. Wang, H. Fu, Y. Nahas, X. Yan, S. Cai, T. Wei, Y. Fang, H. Liu, D. Ji, W. Guo, Z. Gu, Y. Yang, P. Wang, L. Bellaiche, Y. Chen, D.i Wu, Y. Nie, X. Pan, *Nature.* **2022**, *603*, 63.
[19] J. Liu, X. Wang, X. Gao, H. Wang, J. Jian, J. Huang, X. Sun, Z. Qi, S. Misra, Z. He, H. Wang, *Appl. Mater. Today.* **2020**, *21*, 100856.
[20] J. Huang, H. Wang, X. Wang, X. Gao, J. Liu, H. Wang, *ACS Appl. Mater. Interfaces.* **2020**, *12*, 39920.

[21] J. Huang, H. Wang, Z. Qi, P. Lu, D. Zhang, B. Zhang, Z. He, H. Wang, *Nano Lett.* **2021**, *21*, 1032.
[22] J. Song, D. Zhang, P. Lu, Y. Zhang, H. Wang, H. Dou, X. Xu, J. Deitz, X. Zhang, H. Wang, *ACS Appl. Mater. Interfaces.* **2023**, *15*, 37810.
[23] J. Huang, X. Wang, N. L. Hogan, S. Wu, P. Lu, Z. Fan, Y. Dai, B. Zeng, R. Starko-Bowes, J. Jian, H. Wang, L. Li, R. P. Prasankumar, D. Yarotski, M. Sheldon, H.-T. Chen, Z. Jacob, X. Zhang, H. Wang, *Adv. Sci.* **2018**, *5*, 1800416.
[24] D. Zhou, G. Jian, Y. Zheng, S. Gong, F. Shi, *Appl. Surf. Sci.* **2011**, *257*, 7621.
[25] J. Yoon, S. Cho, J.-H. Kim, J. Lee, Z. Bi, A. Serquis, X. Zhang, A. Manthiram, H. Wang, *Adv. Funct. Mater.* **2009**, *19*, 3868.
[26] R. Wu, C. Yun, X. Wang, P. Lu, W. Li, Y. Lin, E.-M. Choi, H. Wang, J. L. MacManus-Driscoll, *ACS Appl. Mater. Interfaces.* **2018**, *10*, 42593.
[27] X. Wang, J. Jian, S. Diaz-Amaya, C. E. Kumah, P. Lu, J. Huang, D. G. Lim, V. G. Pol, J. P. Youngblood, A. Boltasseva, L. A. Stanciu, D. M. O'Carroll, X. Zhang, H. Wang, *Nanoscale Adv.* **2018**, *1*, 1045.
[28] D. Zhang, P. Lu, S. Misra, A. Wissel, Z. He, Z. Qi, X. Gao, X. Sun, J. Liu, J. Lu, X. Zhang, H. Wang, *Adv. Opt. Mater.* **2020**, *9*.
[29] X. Wang, J. Jian, H. Wang, J. Liu, Y. Pachaury, P. Lu, B. X. Rutherford, X. Gao, X. Xu, A. El-Azab, X. Zhang, H. Wang, *Small* **2021**, *17*.
[30] S. Misra, H. Wang, *Mater. Horiz.* **2021**, *8*, 869.
[31] K.-I.l Park, S. Xu, Y. Liu, G.-T. Hwang, S.-J. L. Kang, Z. L. Wang, K. J. Lee, *Nano Lett.* **2010**, *10*, 4939.
[32] D. Zhang, S. Misra, L. Li, X. Wang, J. Jian, P. Lu, X. Gao, X. Sun, Z. Qi, M. Kalaswad, X. Zhang, H. Wang, *Adv. Opt. Mater.* **2020**, *8*, 1901359.
[33] J. Huang, J. L. MacManus-Driscoll, H. Wang, *J. Mater. Res.* **2017**, *32*, 4054.
[34] D.i Lu, D. J. Baek, S. S. Hong, L. F. Kourkoutis, Y. Hikita, H. Y. Hwang, *Nat. Mater.* **2016**, *15*, 1255.
[35] F. M. Chiabrera, S. Yun, Y. Li, R. T. Dahm, H. Zhang, C. K. R. Kirchert, D. V. Christensen, F. Trier, T. S. Jespersen, N. Pryds, Annalen der Physik **2022**, *534*, 2200084.
[36] B. Zhang, J. Huang, B. X. Rutherford, P. Lu, S. Misra, M. Kalaswad, Z. He, X. Gao, X. Sun, L. Li, H. Wang, *Mater. Today Nano.* **2020**, *11*, 100083.
[37] D. Zhang, P. Lu, S. Misra, A. Wissel, Z. He, Z. Qi, X. Gao, X. Sun, J. Liu, J. Lu, X. Zhang, H. Wang, *Adv. Opt. Mater.* **2021**, *9*, 2001154.
[38] B. Zhang, C. Yun, J. L. MacManus-Driscoll, *Nano-Micro Lett.* **2021**, *13*, 39.
[39] S. R. Bakaul, S. Prokhorenko, Q. Zhang, Y. Nahas, Y. Hu, A. Petford-Long, L. Bellaiche, N. Valanoor, *Adv. Mater.* **2021**, *33*, 2105432.
[40] J. Zhang, T. Lin, A. Wang, X. Wang, Q. He, H. Ye, J. Lu, Q. Wang, Z. Liang, F. Jin, S. Chen, M. Fan, E.-J. Guo, Q. Zhang, L. Gu, Z. Luo, L. Si, W. Wu, L. Wang, *Science* **2024**, *383*, 388.
[41] H. Liu, H. Yuan, G. Dong, K. Wu, G. Liu, J. Sun, Z. Zhou, M. Liu, *Adv. Mater. Interface* **2022**, *9*, 2102316.
[42] G. Dong, S. Li, T. Li, H. Wu, T. Nan, X. Wang, H. Liu, Y. Cheng, Y. Zhou, W. Qu, Y. Zhao, B. Peng, Z. Wang, Z. Hu, Z. Luo, W. Ren, S. J. Pennycook, J. Li, J. Sun, Z.-G. Ye, Z. Jiang, Z. Zhou, X. Ding, T. Min, M. Liu, *Adv. Mater.* **2020**, *32*, 2004477.
[43] D. J. Baek, D. Lu, Y. Hikita, H. Y. Hwang, L. F. Kourkoutis, *APL Mater.* **2017**, *5*, 096108.
[44] L. Han, G. Dong, M. Liu, Y. Nie, *Adv. Funct. Mater.* **2024**, *34*, 2309543.
[45] S. Gong, W. Cheng, *Adv. Electron. Mater.* **2017**, *3*, 1600314.
[46] S. Cai, Y. Lun, D. Ji, P. Lv, L.u Han, C. Guo, Y. Zang, S.i Gao, Y. Wei, M. Gu, C. Zhang, Z. Gu, X. Wang, C. Addiego, D. Fang, Y. Nie, J. Hong, P. Wang, X. Pan, *Nat. Commun.* **2022**, *13*, 5116.
[47] X. Lu, Z. Chen, Y.e Cao, Y. Tang, R. Xu, S. Saremi, Z. Zhang, L.u You, Y. Dong, S. Das, H. Zhang, L. Zheng, H. Wu, W. Lv, G. Xie, X. Liu, J. Li, L. Chen, L.-Q. Chen, W. Cao, L. W. Martin, *Nat. Commun.* **2019**, *10*, 3951.
[48] F. Griggio, S. Jesse, A. Kumar, O. Ovchinnikov, H. Kim, T. N. Jackson, D. Damjanovic, S. V. Kalinin, S. Trolier-McKinstry, *Phys. Rev. Lett.* **2012**, *108*, 157604.
[49] V. Nagarajan, A. Roytburd, A. Stanishevsky, S. Prasertchoung, T. Zhao, L. Chen, J. Melngailis, O. Auciello, R. Ramesh, *Nat. Mater.* **2003**, *2*, 43.
[50] B. Wu, A. Heidelberg, J. J. Boland, *Nat. Mater.* **2005**, *4*, 525.
[51] A. Heidelberg, L. T. Ngo, B. Wu, M. A. Phillips, S. Sharma, T. I. Kamins, J. E. Sader, J. J. Boland, *Nano Lett.* **2006**, *6*, 1101.
[52] G.-T. Hwang, H. Park, J.-H. Lee, S. Oh, K.-I. Park, M. Byun, H. Park, G. Ahn, C. K. Jeong, K. No, H. Kwon, S.-G. Lee, B. Joung, K. J. Lee, *Adv. Mater.* **2014**, *26*, 4880.
[53] J. Langer, D. Jimenez de Aberasturi, J. Aizpurua, R. A. Alvarez-Puebla, B. Auguié, J. J. Baumberg, G. C. Bazan, S. E. J. Bell, A. Boisen, A. G. Brolo, J. Choo, D. Cialla-May, V. Deckert, L. Fabris, K. Faulds, F. J. García de Abajo, R. Goodacre, D. Graham, A. J. Haes, C. L. Haynes, C. Huck, T. Itoh, M. Käll, J. Kneipp, N. A. Kotov, H. Kuang, E. C. Le Ru, H. K. Lee, J.-F. Li, X. Y. Ling, et al., *ACS Nano.* **2020**, *14*, 28.
[54] Y. Yu, J. Li, S. A. Solomon, J. Min, J. Tu, W. Guo, C. Xu, Y.u Song, W. Gao, *Sci. Rob.* **2022**, *7*, eabn0495.
[55] C. Hou, H. Wang, Q. Zhang, Y. Li, M. Zhu, *Adv. Mater.* **2014**, *26*, 5018.
[56] J. Luo, L. Zhang, T. Wu, H. Song, C. Tang, *Extreme Mech. Lett.* **2021**, *48*, 101279.
[57] S. Lin, W. Hasi, X. Lin, S. Han, T. Xiang, S. Liang, L.i Wang, *ACS Sens.* **2020**, *5*, 1465.
[58] S. E. Hunyadi, C. J. Murphy, *J. Mater. Chem.* **2006**, *16*, 3929.
[59] U. Mogera, H. Guo, M. Namkoong, M.d S. Rahman, T. Nguyen, L. Tian, *Sci. Adv.* **2022**, *8*, eabn1736.
[60] J. Liu, X. Wang, H. Wang, Z. Qi, J. P. Barnard, B. Zhang, H. Wang, *ACS Appl. Electron. Mater.* **2022**, *4*, 4077.
[61] A. Kursumovic, E. Defay, O. J. Lee, C.-F. Tsai, Z. Bi, H. Wang, J. L. MacManus-Driscoll, *Adv. Funct. Mater.* **2013**, *23*, 5881.
[62] S. Yun, T. E. le Cozannet, C. H. Christoffersen, E. Brand, T. S. Jespersen, N. Pryds, *Small.* **2024**, *20*, 2310782.